Vaporization of perfluorocarbon droplets using optical irradiation

Eric Strohm,[1] Min Rui,[1] Ivan Gorelikov,[2] Naomi Matsuura,[2] and Michael Kolios[1,*]

[1]*Department of Physics, Ryerson University, Toronto, Ontario M5B 2K3, Canada*
[2]*Imaging Research, Sunnybrook Health Sciences Centre, Toronto, Ontario M4N 3M5, Canada*
**mkolios@ryerson.ca*

Abstract: Micron-sized liquid perfluorocarbon (PFC) droplets are currently being investigated as activatable agents for medical imaging and cancer therapy. After injection into the bloodstream, superheated PFC droplets can be vaporized to a gas phase for ultrasound imaging, or for cancer therapy via targeted drug delivery and vessel occlusion. Droplet vaporization has been previously demonstrated using acoustic methods. We propose using laser irradiation as a means to induce PFC droplet vaporization using a method we term optical droplet vaporization (ODV). In order to facilitate ODV of PFC droplets which have negligible absorption in the infrared spectrum, optical absorbing nanoparticles were incorporated into the droplet. In this study, micron-sized PFC droplets loaded with silica-coated lead sulfide (PbS) nanoparticles were evaluated using a 1064 nm laser and ultra-high frequency photoacoustic ultrasound (at 200 and 375 MHz). The photoacoustic response was proportional to nanoparticle loading and successful optical droplet vaporization of individual PFC droplets was confirmed using photoacoustic, acoustic, and optical measurements. A minimum laser fluence of 1.4 J/cm^2 was required to vaporize the droplets. The vaporization of PFC droplets via laser irradiation can lead to the activation of PFC agents in tissues previously not accessible using standard ultrasound-based techniques.

OCIS codes: (170.5120) Photoacoustic imaging; (170.3880) Medical and biological imaging

References and links

1. C. S. Cohn and M. M. Cushing, "Oxygen therapeutics: perfluorocarbons and blood substitute safety," Crit. Care Clin. **25**(2), 399–414 (2009).
2. M. Behan, D. O'Connell, R. F. Mattrey, and D. N. Carney, "Perfluorooctylbromide as a contrast agent for CT and sonography: preliminary clinical results," AJR Am. J. Roentgenol. **160**(2), 399–405 (1993).
3. R. F. Mattrey, P. C. Hajek, V. M. Gylys-Morin, L. L. Baker, J. Martin, D. C. Long, and D. M. Long, "Perfluorochemicals as gastrointestinal contrast agents for MR imaging: preliminary studies in rats and humans," AJR Am. J. Roentgenol. **148**(6), 1259–1263 (1987).
4. N. Matsuura, R. Williams, I. Gorelikov, J. Chaudhuri, J. Rowlands, K. Hynynen, S. Foster, P. Burns, and N. Resnik, "Nanoparticle-loaded perfluorocarbon droplets for imaging and therapy," in *Proceedings of the IEEE Ultrasonics Symposium* (IEEE, New York, 2009), pp. 5–8.
5. J. G. Riess and M. LeBlanc, "Solubility and transport phenomena in perfluorochemicals relevant to blood substitution and other biomedical applications," Pure Appl. Chem. **54**(12), 2383–2406 (1982).
6. M. L. Fabiilli, K. J. Haworth, I. E. Sebastian, O. D. Kripfgans, P. L. Carson, and J. B. Fowlkes, "Delivery of chlorambucil using an acoustically-triggered perfluoropentane emulsion," Ultrasound Med. Biol. **36**(8), 1364–1375 (2010).
7. O. D. Kripfgans, J. B. Fowlkes, M. Woydt, O. P. Eldevik, and P. L. Carson, "In vivo droplet vaporization for occlusion therapy and phase aberration correction," IEEE Trans. Ultrason. Ferroelectr. Freq. Control **49**(6), 726–738 (2002).
8. T. Giesecke and K. Hynynen, "Ultrasound-mediated cavitation thresholds of liquid perfluorocarbon droplets in vitro," Ultrasound Med. Biol. **29**(9), 1359–1365 (2003).
9. E. C. Unger, T. Porter, W. Culp, R. Labell, T. Matsunaga, and R. Zutshi, "Therapeutic applications of lipid-coated microbubbles," Adv. Drug Deliv. Rev. **56**(9), 1291–1314 (2004).
10. O. D. Kripfgans, J. B. Fowlkes, D. L. Miller, O. P. Eldevik, and P. L. Carson, "Acoustic droplet vaporization for therapeutic and diagnostic applications," Ultrasound Med. Biol. **26**(7), 1177–1189 (2000).

#144029 - $15.00 USDv Received 14 Mar 2011; revised 14 Apr 2011; accepted 26 Apr 2011; published 4 May 2011

11. M. Zhang, M. L. Fabiilli, K. J. Haworth, J. B. Fowlkes, O. D. Kripfgans, W. W. Roberts, K. A. Ives, and P. L. Carson, "Initial investigation of acoustic droplet vaporization for occlusion in canine kidney," Ultrasound Med. Biol. **36**(10), 1691–1703 (2010).
12. W. L. J. Hasi, Z. W. Lu, S. Gong, S. J. Liu, Q. Li, and W. M. He, "Investigation of stimulated Brillouin scattering media perfluoro-compound and perfluoropolyether with a low absorption coefficient and high power-load ability," Appl. Opt. **47**(7), 1010–1014 (2008).
13. G. J. Diebold, T. Sun, and M. I. Khan, "Photoacoustic monopole radiation in one, two, and three dimensions," Phys. Rev. Lett. **67**(24), 3384–3387 (1991).
14. E. M. Strohm, M. Rui, I. Gorelikov, N. Matsuura, and M. Kolios, "Optical droplet vaporization of micron-sized perfluorocarbon droplets and their photoacoustic detection," Proc. SPIE **7899**, 78993H, 78993H-7 (2011).
15. G. Paltauf and P. E. Dyer, "Photomechanical processes and effects in ablation," Chem. Rev. **103**(2), 487–518 (2003).
16. M. A. Hines and G. D. Scholes, "Colloidal PbS nanocrystals with size-tunable near-infrared emission: observation of post-synthesis self-narrowing of the particle size distribution," Adv. Mater. (Deerfield Beach Fla.) **15**(21), 1844–1849 (2003).
17. I. Gorelikov and N. Matsuura, "Single-step coating of mesoporous silica on cetyltrimethyl ammonium bromide-capped nanoparticles," Nano Lett. **8**(1), 369–373 (2008).
18. D. K. Yi, S. T. Selvan, S. S. Lee, G. C. Papaefthymiou, D. Kundaliya, and J. Y. Ying, "Silica-coated nanocomposites of magnetic nanoparticles and quantum dots," J. Am. Chem. Soc. **127**(14), 4990–4991 (2005).
19. N. Matsuura, I. Gorelikov, R. Williams, K. Wan, S. Zhu, J. Booth, P. Burns, K. Hynynen, and J. A. Rowlands, "Nanoparticle-tagged perfluorocarbon droplets for medical imaging," Mater. Res. Soc. Symp. Proc. **1140**, 1–6 (2009).
20. M. Rui, S. Narashimhan, W. Bost, F. Stracke, E. Weiss, R. Lemor, and M. C. Kolios, "Gigahertz optoacoustic imaging for cellular imaging," Proc. SPIE **7564**, 756411, 756411-6 (2010).
21. E. M. Strohm, G. J. Czarnota, and M. C. Kolios, "Quantitative measurements of apoptotic cell properties using acoustic microscopy," IEEE Trans. Ultrason. Ferroelectr. Freq. Control **57**(10), 2293–2304 (2010).
22. J. N. Marsh, C. S. Hall, S. A. Wickline, and G. M. Lanza, "Temperature dependence of acoustic impedance for specific fluorocarbon liquids," J. Acoust. Soc. Am. **112**(6), 2858–2862 (2002).
23. V. S. Ardebili, A. N. Sinclair, and J. K. Spelt, "Ultrasonic couplants for acoustic microscopy of low speed materials," IEEE Trans. Ultrason. Ferroelectr. Freq. Control **44**(1), 102–107 (1997).
24. Z. Z. Wong, O. D. Kripfgans, A. Qamar, J. B. Fowlkes, and J. L. Bull, "Bubble evolution in acoustic droplet vaporization at physiological temperature via ultra-high speed imaging," Soft Matter **7**(8), 4009–4016 (2011).
25. E. M. Strohm, M. C. Kolios, I. Gorelikov, and N. Matsuura, "Optical droplet vaporization (ODV): photoacoustic characterization of perfluorocarbon droplets," in *Proceedings of the IEEE Ultrasonics Symposium* (IEEE, New York, 2010) (to be published).

1. Introduction

Perfluorocarbons (PFCs) are non-toxic, chemically and biologically inert compounds [1] with unique physical properties that enable their use in a wide range of medical applications. Applications include using PFCs as contrast agents in X-ray computed tomography [2], magnetic resonance imaging [3] and ultrasound imaging [4], as blood substitutes [5], and for cancer therapy via targeted drug delivery [6] and vessel occlusion [7].

PFC droplets made from perfluoropentane (PFP, C_5F_{12}) are currently being investigated as externally activatable contrast agents for the detection and treatment of cancer. Despite its low boiling point (29°C at 1 atm), micron-sized (1-5 μm) PFP droplets can circulate within the body in a superheated state [8] after intravenous injection. PFP droplets have poor ultrasound contrast due to their acoustic impedance which is similar to that of the surrounding tissue, therefore droplets must be converted to gas bubbles to enable their use as an effective ultrasound contrast agent. In therapeutic applications, the increase in the droplet volume upon conversion to a bubble has been used to occlude blood vessels [7], and the droplets can also be used as drug delivery vehicles [9]. Typically, the conversion from droplets to bubbles is induced via ultrasound irradiation once a threshold pressure is achieved [10]. In this approach however, large peak negative ultrasonic pressures that may be harmful to normal surrounding tissue (e.g., 10 to 13 MPa at approximately 3.0 MHz in canine kidney [11]) have been reported during transcutaneous acoustic droplet conversion (ADV). Also, ultrasound beams cannot effectively penetrate gaseous enclosures in the human body, such as the lungs. Therefore, another method is required to induce the therapeutic function of the droplets in these locations.

We suggest using laser light to activate the droplets. Near-infrared light is well-suited to medical imaging and therapy, as this wavelength range has good tissue penetration depth and results in low photoacoustic background signals from tissue and blood in-vivo. The use of

#144029 - $15.00 USDv Received 14 Mar 2011; revised 14 Apr 2011; accepted 26 Apr 2011; published 4 May 2011

laser light allows droplet activation at locations that light can be delivered but ultrasound could not. Moreover, a judicious choice of laser wavelength and light absorbing structure could offer the opportunity for the droplet to be used either as a photoacoustic contrast agent and/or as a therapeutic agent. For example, different optical absorbers with different absorption coefficients could be used so that one wavelength induces a photoacoustic signal, while another triggers vaporization. Pulse-echo acoustic measurements could be used after vaporization to detect the location and/or number of the formed bubbles. PFC droplets could therefore be used as a dual-contrast agent for contrast enhanced imaging and/or cancer therapy: using photoacoustic imaging to determine the locations of the agents before the therapeutic intervention, and then ultrasound imaging after the payload delivery (provided that an acoustic path is available). However, liquid PFC has negligible absorption in the infrared region of the spectrum [12] and laser-induced optical droplet vaporization (ODV) is not possible. Thus, we propose to facilitate ODV by incorporating infrared absorbing PbS nanoparticles into PFC droplets. PbS nanoparticles are introduced in this study, however nanoparticles made of other optical absorbing materials, such as gold, iron oxide or carbon, could potentially be used.

In this paper we demonstrate that a photoacoustic signal can be measured from micron-sized PFC droplets containing PbS nanoparticles before vaporization. The photoacoustic signal of droplets made with two different nanoparticle concentrations was correlated to the droplet absorption coefficient, showing that the absorption coefficient can be controlled by the amount of nanoparticles used during droplet manufacturing. We then demonstrate that laser light may be used to vaporize nanoparticle-loaded PFC droplets when irradiated above a threshold laser fluence, and confirm that the resulting bubbles can be detected via ultrasound methods.

2. Theory

Liquid PFC droplets are optically transparent and have negligible absorption in the infrared spectrum, therefore optically absorbing nanoparticles must be incorporated into the droplet to facilitate adequate energy absorption. When irradiated by a pulsed laser, the nanoparticles undergo a rapid temperature increase, which subsequently heat the surrounding PFC liquid while simultaneously producing an ultrasound pressure wave (the photoacoustic signal). We assume a uniform distribution of nanoparticles within the droplet, and the droplet is optically transparent to allow equal and instantaneous heating of each nanoparticle. Moreover, we assume that the entire droplet will undergo a rapid uniform thermoelastic expansion. The pressure resulting from the expansion of a spherical liquid droplet is [13]

$$p(q) = \mu_a I_0 A(q), \tag{1}$$

where

$$A(q) = \frac{iac_d\beta}{C_p(r/a)} e^{-iq\tau} \frac{(\sin q - q\cos q)/q^2}{(1-\rho)(\sin q/q) - \cos q + ic\rho \sin q}, \tag{2}$$

where μ_a is the droplet absorption coefficient, I_0 is the laser intensity, a is the droplet radius, c_d is the sound velocity in the droplet, C_p is the heat capacity, β is the thermal expansion coefficient, and ρ and c are the ratios of the density and sound velocity between the droplet and coupling fluid, respectively. The time τ and frequency q are redefined as dimensionless quantities where $q = 2\pi fa/c_d$ and $\tau = (v/a)[t-(r-a)/c_f]$ is the delay time from the radius of the droplet, where c_f is the sound velocity in the coupling fluid [13]. In Eq. (1), the photoacoustic pressure amplitude depends on the combined effects of the bulk properties of the droplet and the effective absorption coefficient μ_a of the droplet. Previous work showed good agreement of the ultrasound spectral features predicted by the model [Eqs. (1) and (2)] and photoacoustic measurements of micron-sized PFC droplets [14]. For efficient photoacoustic signal

#144029 - $15.00 USDv Received 14 Mar 2011; revised 14 Apr 2011; accepted 26 Apr 2011; published 4 May 2011

generation, the pulse width τ must be less than the stress and thermal confinement times, which are given as

$$t_{stress} = \frac{d}{c_d}, \quad t_{thermal} = \frac{d^2}{4\alpha}, \tag{3}$$

where d is the diameter and α is the thermal diffusivity of the droplet [15]. For a typical 1 μm diameter liquid perfluorocarbon droplet, the thermal and stress confinement times are approximately 8 μs and 2 ns, respectively. The pulse duration used in these experiments is less than 2 ns, therefore the thermal and stress confinement conditions have been satisfied.

3. Method

3.1. PFC emulsions

Monodisperse PbS nanoparticles were synthesized [16], coated with silica [17], [18], and fluorinated for miscibilization into PFP (Synquest) [19]. All chemicals for silica-coated nanoparticle synthesis and PFP solubilization were purchased from Sigma-Aldrich, and used as-received. Micrometer-scale, PbS-loaded PFP droplets were prepared using 5 mL deionized water, 0.15 mL PbS-PFP/PFP solution, and 0.03 mL anionic fluorosurfactant (Zonyl FSP, Sigma-Aldrich) via emulsification using polymer membranes (Whatman, 10 micron pore size), following coarse emulsification by vortexing.

PbS nanoparticles were imaged using a Hitachi HD-2000 scanning transmission electron microscope (TEM). PFC droplet sizes were measured using a Multisizer III Coulter counter (Beckman Coulter Inc., Fullerton, CA). The absorption coefficient of PbS-loaded PFP was determined using a Cary 6000i UV-vis-NIR spectrophotometer. PbS concentration of the PFP solution was determined using an Optima 3000 inductively coupled plasma atomic emission spectroscopy (ICP-AES) system.

3.2. *Photoacoustic microscope*

A modified SASAM 1000 scanning acoustic microscope (Kibero GmbH, Germany) was used for these experiments. It consists of an Olympus IX81 inverted optical microscope (Olympus, Japan) outfitted with an acoustic module installed above the optical objective for ultrasound measurements. A 1064 nm laser (Teem Photonics, France) was collimated through the back port of the microscope and focused onto the sample, allowing for simultaneous optical and photoacoustic measurements. Details of the system construction can be found elsewhere [20], [21].

The laser was focused to a 4 μm spot size using a 10x objective with a 0.3 numerical aperture, giving a laser fluence of up to 3.8 J/cm^2 per pulse. The laser had a pulse width of 700 ps with an adjustable repetition frequency of up to 2 kHz. This laser was used for both the photoacoustic imaging and droplet vaporization. Two transducers were used for the acoustic and photoacoustic measurements. The 200 MHz transducer had a 60° aperture angle and −6 dB bandwidth of 45%, while the 375 MHz transducer had a 60° aperture angle and a −6 dB bandwidth of 42%.

All photoacoustic and ultrasound measurements were amplified by a 40 dB amplifier (Miteq, USA) and digitized at a rate of 8 GHz (Acqiris, USA). For the ultrasound pulse-echo measurements, 10 V_{pp} pulses were generated at a pulse repetition frequency of up to 500 kHz using a monocycle pulse generator with a center frequency of 300 MHz and 100% bandwidth. For photoacoustic measurements, the transducers were used passively to record the photoacoustic signals by synchronizing the receiver to the laser pulse. The overall pulse repetition frequency in photoacoustic mode was limited by the repetition frequency of the laser, which was 2 kHz. 100-200 signals were averaged for each measurement to increase the signal-noise ratio (SNR). The signals were then passed through a 110-800 MHz software bandpass filter to remove noise and enhance the SNR.

#144029 - $15.00 USDv Received 14 Mar 2011; revised 14 Apr 2011; accepted 26 Apr 2011; published 4 May 2011

3.3. Measurements

Droplets were diluted with water in a chamber slide (Nunc, Germany). The droplet concentration was diluted to ensure that droplets were sufficiently far apart from each other to probe them individually. The diameter of a single droplet was measured using the images recorded by the optical microscope and then each droplet was centered under the transducer. The laser and transducer were aligned for photoacoustic measurements. The transducer and laser position was kept constant while the microscope stage was scanned over a 15x15 μm area using a 0.5 μm step size, with the droplet located at the center. The laser fluence was increased, and the process repeated until vaporization occurred or the maximum laser fluence level was reached.

PbS-loaded PFP droplets were measured at two different nanoparticle loading levels, designated "low" and "high". The high loading contained double the nanoparticles of the low loading. Ten droplets were measured at each PbS loading level using two transducer frequencies, 200 and 375 MHz, for a total of 40 droplet measurements. Droplets were grouped into two categories, small (2-4 μm) and large (4-7 μm). A laser fluence ranging from 0.05 J/cm^2 to 3.4 J/cm^2 was used, measured at the focal point using a Nova II laser power meter (Ophir, USA).

The envelope of the signal at each x-y position of a single droplet was found by using the Hilbert transform of the recorded ultrasound data, from which the maximum signal amplitude was determined. Assuming the bulk droplet properties do not change with laser fluence, $A(q)$ in Eq. (1) is constant. Therefore for a droplet irradiated with a known fluence F, Eq. (1) can be rewritten as

$$p(q) = B(q)F, \tag{4}$$

where $B(q)$ is constant at a specific frequency. Assuming $A(q)$ is constant over the laser fluence range used, and the temperature increase over time was negligible, $B(q)$ is the slope of the photoacoustic pressure measured as a function of laser fluence. In our measurements, the slope has units of V cm^2/J. The photoacoustic signal detected is proportional to pressure. Therefore, if the conversion factor between the voltage and pressure for the transducer was known, the slope would be proportional to the absorption coefficient μ_a, with units of cm^{-1}.

C-scan images were made by quantizing the maximum photoacoustic signal from each x-y position of each droplet over an entire fluence range to grayscale values. The largest signal amplitude was assigned white, while the lowest signal amplitude was assigned black. The same dynamic range was used for all images.

All measurements were made at 36°C to simulate physiological conditions within the human body. Occasionally bubbles would become dislodged from the substrate and float to the surface, therefore the transducer was examined after each droplet vaporization to ensure a bubble did not become lodged in the transducer cavity, which would strongly attenuate the ultrasound signals.

4. Results

4.1. Droplet configuration

In this study, PbS nanoparticles were selected as the absorbing nanoparticle for integration into PFP, due to their high absorption coefficient in the infrared, ease of synthesis, and small size permitting high-yield incorporation into micron-scale PFP droplets. TEM images demonstrate good monodispersity of silica-coated PbS nanoparticles (10 nm in diameter, which included a 5 nm PbS core and a 2.5 nm thick silica shell, Fig. 1A), after miscibilization into PFP. The absorption coefficient of the PbS-loaded PFC solutions was 2.07 cm^{-1} at low PbS loading, and 4.31 cm^{-1} at high PbS loading at 1064 nm (Fig. 1B), measured using a spectrophotometer. The ratio of the measured absorption coefficient at low and high PbS loadings for droplets in suspension was therefore 0.48.

#144029 - $15.00 USDv Received 14 Mar 2011; revised 14 Apr 2011; accepted 26 Apr 2011; published 4 May 2011

The PbS concentration within the PbS-loaded PFP droplets was 7.16 mg/mL of PFC at low PbS loading, and 15.1 mg/mL PFC at high PbS loading as measured by ICP-AES, giving a low-high PbS loading ratio of 0.47, similar to the ratio determined using the absorption coefficients.

The droplets in suspension ranged in diameter from approximately 1-12 µm, measured using a Multisizer III Coulter Counter. In the photoacoustic microscope, individual droplet diameters were determined optically. However poor optical contrast made it difficult to accurately measure the diameter of small droplets, therefore droplets below approximately 2 µm in diameter were not used in this study. Only droplets with diameters between 2 and 7 µm were used for these experiments.

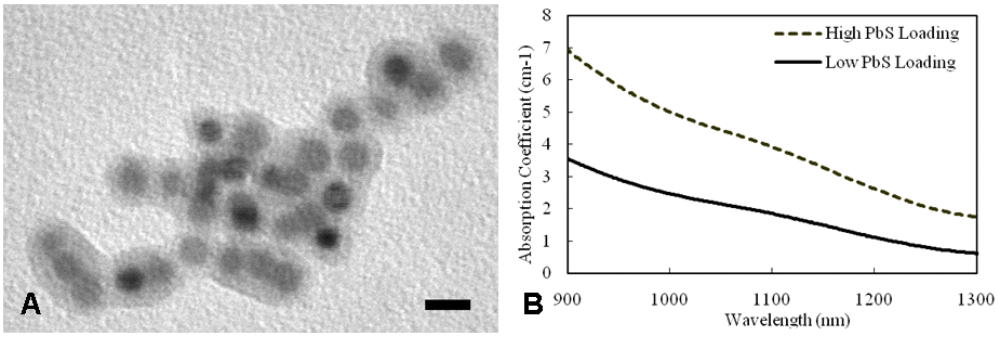

Fig. 1. (A) A TEM image of silica-coated PbS nanoparticles after miscibilization into PFC. The PbS nanoparticles were approximately 10 nm in diameter, composed of a 5 nm PbS core and a 2.5 nm silica shell. The scale bar is 10 nm. (B) The absorption spectrum of droplets at low PbS loading (2.07 cm^{-1} at 1064 nm, solid line) and high PbS loading (4.31 cm^{-1} at 1064 nm, dotted line).

4.2. Photoacoustic signals

The photoacoustic signal c-scan of a single 6.9 µm diameter droplet with high PbS loading, measured at 200 MHz as a function of laser fluence is shown in Fig. 2. The signal amplitude increased with increasing laser fluence, until vaporization occurred in the last frame. The exact point of vaporization could be determined in the final frame (as indicated by the arrow), as no signal was detected following vaporization. No photoacoustic signal was detected from the resulting bubbles after vaporization. In addition, no photoacoustic signal was detected from unloaded PFP droplets at the fluences used.

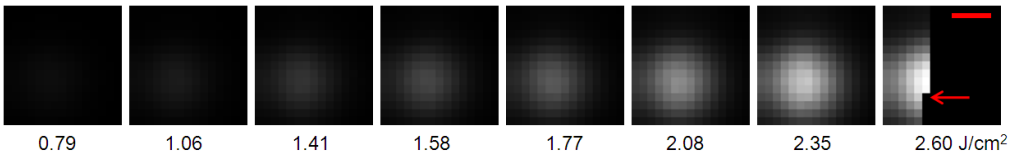

Fig. 2. Photoacoustic c-scan image sequence of a single 6.9 µm droplet with high PbS loading as a function of laser fluence, measured at 200 MHz. Intensity was normalized to maximum amplitude across all measurements and the same dynamic range was used for all images. An increase in the photoacoustic signal was observed with increasing laser fluence, until vaporization occurred in the last frame as indicated by the arrow. The scale bar is 2.5 µm and is the same for all images.

The photoacoustic signal amplitude from PFP droplets containing PbS nanoparticles was measured using 200 and 375 MHz transducers, at two different nanoparticle concentrations (low and high) and over a laser fluence range of 0.05 to 3.4 J/cm^2 using approximately a 0.25 J/cm^2 step size. The signal amplitude was obtained from the central region of each droplet. The slope of the photoacoustic signal vs. laser fluence is proportional to the absorption coefficient μ_a, as shown in Eq. (4). The measured photoacoustic signal vs. laser fluence for the

#144029 - $15.00 USDv Received 14 Mar 2011; revised 14 Apr 2011; accepted 26 Apr 2011; published 4 May 2011

200 and 375 MHz transducers at two different PbS loadings are shown in Figs. 3A-3D. Some non-linearity was observed above approximately 2.0 J/cm^2, therefore these measurements were not included in the slope calculations.

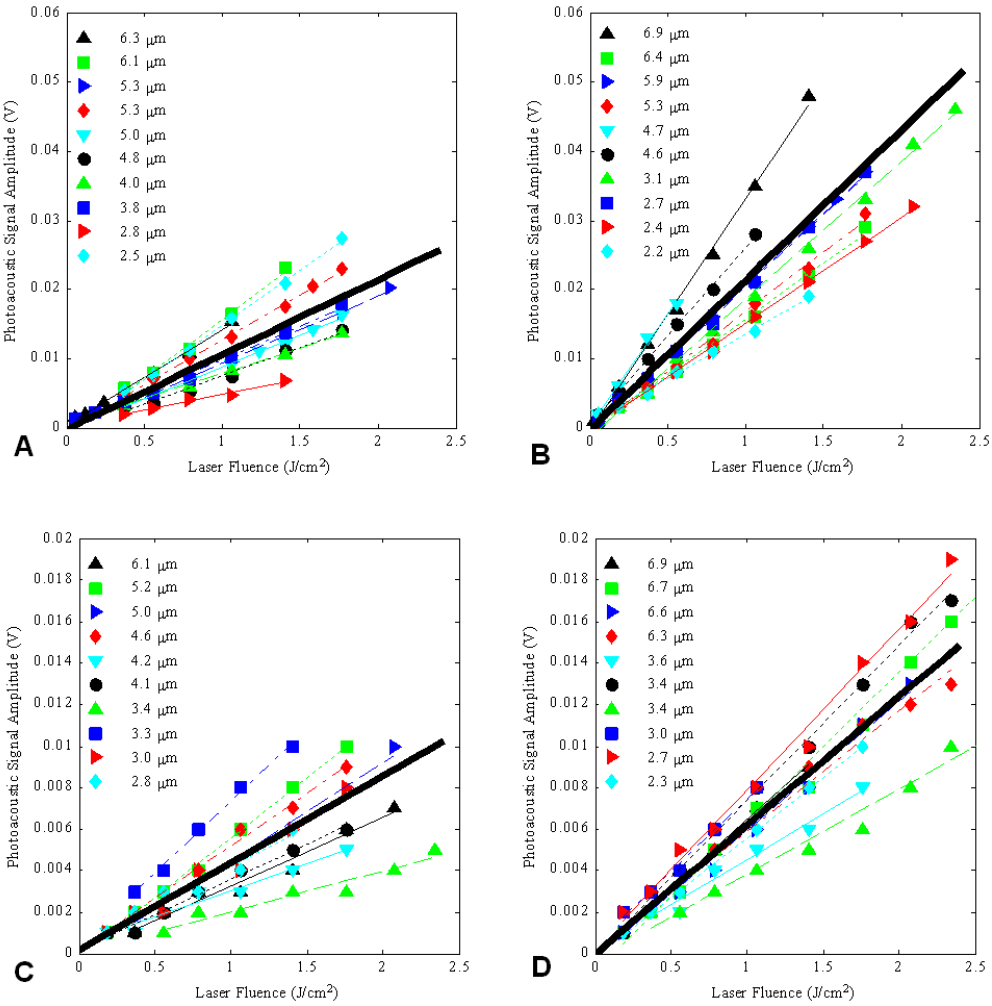

Fig. 3. The photoacoustic signal vs. laser fluence for droplets measured at (A) low PbS loading at 200 MHz, (B) high PbS loading at 200 MHz, (C) low PbS loading at 375 MHz, and (D) high PbS loading at 375 MHz. A line of best fit is shown for each droplet, and the average slope is shown by the thick black line.

Ten droplets were measured at each droplet configuration (low and high PbS loading at 200 MHz, and low and high PbS loading at 375 MHz) for a total of forty droplets. The average slope over ten measurements is shown in Table 1 with standard deviation. The slope at low and high PbS loading was 0.0108 ± 0.0040 V cm^2/J and 0.0216 ± 0.0072 V cm^2/J at 200 MHz, respectively, and 0.0042 ± 0.0017 V cm^2/J and 0.0062 ± 0.0013 V cm^2/J at 375 MHz, respectively. The ratio of the slope at low and high PbS loadings was 0.50 at 200 MHz, and 0.68 at 375 MHz. The effect of droplet size on the slope was investigated by averaging the slope for small (2-4 µm) and large (4-7 µm) droplets. The ratio of the slope at low and high PbS loadings at 200 MHz was 0.52 for small droplets and 0.46 for large droplets, while the ratio at 375 MHz was 0.72 for small droplets and 0.65 for large droplets. These results are summarized in Table 1.

#144029 - $15.00 USDv Received 14 Mar 2011; revised 14 Apr 2011; accepted 26 Apr 2011; published 4 May 2011

Table 1. Slope Calculation vs. Droplet Concentration and Ultrasound Frequency

Nanoparticle Loading	Frequency (MHz)	Slope (V cm^2/J) All droplets	Slope (V cm^2/J) 2-4 µm droplets	Slope (V cm^2/J) 4-7 µm droplets
Low	200	0.0108 ± 0.0040	0.0100 ± 0.0057	0.0111 ± 0.0035
High	200	0.0216 ± 0.0072	0.0190 ± 0.0051	0.0242 ± 0.0085
Low	375	0.0042 ± 0.0017	0.0044 ± 0.0023	0.0041 ± 0.0013
High	375	0.0062 ± 0.0013	0.0061 ± 0.0016	0.0062 ± 0.0005
Slope ratio Low-high loading	200	0.50	0.52	0.46
Slope ratio Low-high loading	375	0.68	0.72	0.65

4.3. Droplet vaporization

Droplet vaporization was confirmed via optical and acoustic methods. Video sequences were recorded during bubble expansion. For one of the droplets, an initial rapid increase in diameter from 4.5 µm to 19.5 µm was measured optically one second after vaporization (Fig. 4), resulting in a radial expansion ratio of 4.3x. After this initial rapid expansion, the bubble diameter slowly increased over time.

Twenty droplets were measured at each low and high PbS loading. Within the fluence thresholds of the experiment, eleven droplets were vaporized at low PbS loading (55%), while sixteen droplets were vaporized at high PbS loading (80%). The mean fluence level required to vaporize droplets at low PbS loading was 2.8 ± 0.5 J/cm^2 (minimum fluence 1.8 J/cm^2), and the mean fluence required to vaporize droplets at high PbS loading was 2.7 ± 0.6 J/cm^2 (minimum fluence 1.4 J/cm^2).

Acoustic pulse echo measurements were made using a 375 MHz transducer to probe the bubble during expansion. The signal from the glass substrate under the droplet was approximately 250 mV while the droplet was in the liquid phase. The signal from the droplet itself was small and obscured within the substrate signal, as the transducers could not resolve the droplet and substrate signal due to the small droplet size. After vaporization, no signal from the substrate was detected; however a strong signal (200-300 mV) from the bubble surface was measured.

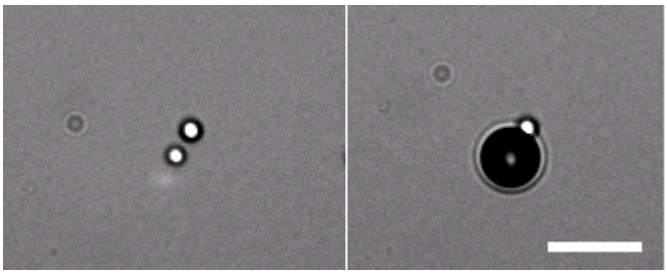

Fig. 4. Droplet vaporization observed via optical microscopy. The initial droplet size was 4.5 µm (left). The bubble size was 19.5 µm one second after vaporization (right). The scale bar is 30 µm.

5. Discussion

5.1. Droplet photoacoustic signals and optical absorption

As discussed in section 3.3, the slope of the photoacoustic signal vs. laser fluence plot in Fig. 3 is proportional to μ_a, assuming the bulk droplet properties remain constant for the laser fluences and number of laser exposures used. Two parameters are required to determine the absorption coefficient directly from the slope calculations. First, the relationship between the measured photoacoustic signal and pressure must be known. It is currently not possible to directly measure the pressure with ultra-high frequency transducers. Second, the variables in $A(q)$ (Eq. (2) must be known at the frequencies and temperature used in this study. The sound velocity of PFC liquids have not been measured at 375 MHz, therefore a direct calculation is

#144029 - $15.00 USDv Received 14 Mar 2011; revised 14 Apr 2011; accepted 26 Apr 2011; published 4 May 2011

not possible. In this work we compared the ratio of the slopes (which are proportional to the absorption coefficient) instead of calculating and comparing the absorption coefficient directly. The ratio of the measured slope between low and high PbS loading should be equal to the ratio of the absorption coefficient between low and high PbS loading measured using a spectrophotometer.

The low-high PbS loading ratio derived from the slope of the experimental measurements [Eq. (1)] was 0.50 at 200 MHz and 0.68 at 375 MHz, as shown in Table 1. The low-high PbS loading ratio was 0.48 determined by measuring the absorption coefficient using a spectrophotometer, and 0.47 determined via ICP. The loading ratio determined via photoacoustic methods agrees with the loading ratio calculated by using the data collected using the 200 MHz transducer, but discrepancies were noted when loading ratio calculated by using the data collected using the 375 MHz transducer (Table 1).

Several assumptions were made during these measurements. It is not known how the PbS nanoparticles affect the bulk PFC properties. Due to the relatively low nanoparticle concentration in the PFC, the volume ratio of the nanoparticles compared to the PFC would be small, and the effect on the sound velocity, heat capacity and coefficient of thermal expansion in Eq. (1) was likely negligible. However it is unknown how the properties vary with ultrasound frequency. The sound velocity of PFC liquids have been measured at 10 MHz [22] and 250 MHz [23], it is unknown what degree of dispersion is present at higher frequencies. Therefore a direct comparison of the results at 200 and 375 MHz was difficult.

There could be several reasons why the slopes calculated using data collected with the 200 and 375 MHz transducers for the same loading are not similar. The sensitivity and SNR of the 200 MHz transducer is higher than the 375 MHz transducer, as observed by the increased signal in the photoacoustic signal of Fig. 3 and percentage standard deviation. While the depth of field of both transducers is large in comparison to the droplet diameter (approximately 70 µm and 40 µm for the 200 and 375 MHz transducers, respectively), the lateral resolution at 200 MHz is 8 µm, in comparison to 4 µm at 375 MHz. Consequently the 375 MHz transducer is more sensitive to the focus position.

Despite the difference in the slope ratio calculation between the two transducers, both measurements showed an increase in the slope, indicating an increase in the absorption coefficient and therefore increase in the optical absorbing agent concentration contained within the droplet.

5.2. Photoacoustic signals from bubbles

Photoacoustic signals were measured from droplets before vaporization as discussed in the previous section. Once the droplet vaporized, no photoacoustic signal was detected. A pressure wave should be generated due to the rapid shell expansion that occurs during the phase change. In our measurements, 100-200 point averaging was used to improve the SNR. Since the pressure wave generated during the rapid expansion is a very fast event, the signal would be greatly reduced due to the RF signal averaging. Methods are currently being investigated to detect this pressure wave.

After vaporization, attempts were made to measure a photoacoustic signal from the bubble using the same method as with the droplets. No photoacoustic signal was detected from the bubbles. In droplet form, the nanoparticles would be suspended within the liquid core. During vaporization, the rapid expansion may force the nanoparticles towards the bubble shell, or possibly expel them outside the bubble. Since the bubble diameter is approximately 5x larger than the initial droplet diameter immediately following vaporization, the change in volume is approximately 125x. Therefore the nanoparticle concentration within the bubble or around the shell may be too dilute to generate a detectable photoacoustic signal.

5.3. Droplet expansion

Two expansion regimes were observed optically during the liquid to gas phase change during vaporization; an initial rapid expansion that occurred within one second, then a slow gradual expansion over a period of minutes. A 4.5 µm diameter droplet expanded to 19.5 µm within

#144029 - $15.00 USDv Received 14 Mar 2011; revised 14 Apr 2011; accepted 26 Apr 2011; published 4 May 2011

one second after vaporization, a 4.3x increase in radial diameter. This expansion ratio is similar to other studies using acoustic droplet vaporization, which have measured a radial increase of 5.3x [10] and 5.05x [24] for vaporization of micron-sized droplets, independent of initial droplet diameter. These experimental results agree with a radial expansion ratio of 5x predicted using ideal gas law calculations [10]. This expansion is likely due to the increase in volume during the liquid to gas phase change. The subsequent slow expansion observed over minutes has been hypothesized to be due to diffusion of gases between the coupling fluid and bubble [10].

Pulse echo measurements were used to verify a liquid-gas phase change after vaporization. The substrate signal under the liquid droplet was approximately 250 mV. After vaporization, a 200-300 mV signal from the bubble surface was measured and the substrate signal was completely attenuated. The strong signal from the bubble surface and attenuation of the substrate signal under the droplet indicate that a phase change from liquid to gas occurred.

5.4. Vaporization mechanism

It is clear by both the change in droplet volume and echogenicity, that the liquid PFC undergoes a phase transition to gas upon laser irradiation above a threshold fluence. The mechanism for optical droplet vaporization is not well understood. Vaporization could be thermally activated, where heating of the nanoparticles locally increases the temperature of the PFC past the boiling point, resulting in vaporization. Alternatively, the method could be acoustically driven, despite using an optical irradiation source. As a photoacoustic signal is detected at the lower fluence, it is known that the nanoparticles act as very small but numerous acoustic sources from within the droplet. The mechanism could be similar to that observed during acoustic droplet vaporization, where above a certain peak negative pressure threshold vaporization occurs [10]. Our future work will examine both acoustic and optical droplet vaporization using the same platform, and could lead to a better understanding of droplet vaporization mechanisms.

In this study, the average fluence required to achieve vaporization was 2.8 ± 0.5 J/cm^2 with low PbS loading and 2.7 ± 0.6 J/cm^2 with high PbS loading. The average fluence was very similar for both loadings, however the minimum fluence level required to achieve droplet vaporization was 1.8 J/cm^2 with low PbS loading and 1.4 J/cm^2 with high PbS loading. There was a higher probability of vaporization at high PbS loading (80%) than low PbS loading (55%). These results suggest that there is a significant variation in the nanoparticle concentration between individual droplets. This is demonstrated by the range of slopes observed in Fig. 3, and the large standard deviation in the average slope calculations. In addition, while the average fluence required for vaporization was similar for both loadings, the standard deviation was relatively high. Despite these variations, the slope ratio between low and high PbS loading averaged over ten droplets showed good agreement with the absorption coefficient ratio measured directly.

Our previous work using a higher nanoparticle concentration achieved vaporization using 0.7 J/cm^2 [25]. By optimizing the optical absorption by changing the nanoparticle type, shape or concentration, lower vaporization fluence thresholds could be realized. Such modifications to nanoparticle composition are underway.

5. Conclusion

We demonstrate in this work a dual-mode contrast agent that can be used for photoacoustic and acoustic measurements. PbS nanoparticles were successfully incorporated into micron-sized PFP droplets and the photoacoustic signal measured with 200 and 375 MHz transducers. The photoacoustic signal generated was proportional to the absorption coefficient of the droplets. The minimum laser fluence required for conversion of the liquid droplet to a bubble (what we term optical droplet vaporization) was 1.4 J/cm^2 for the nanoparticle type and configuration presented here, however vaporization was not achieved for all droplets. Vaporization was confirmed by an increase in the ultrasound backscatter from the bubble

#144029 - $15.00 USDv Received 14 Mar 2011; revised 14 Apr 2011; accepted 26 Apr 2011; published 4 May 2011

surface and attenuation of the substrate signal through the bubble, as compared to the liquid droplet.

Acknowledgments

E. Strohm is supported through a PGS-D NSERC doctoral scholarship. This research was undertaken, in part, thanks to funding from the Canada Research Chairs Program and NSERC awarded to M. Kolios. Funding to purchase the equipment was provided by the Canada Foundation for Innovation, the Ontario Ministry of Research and Innovation, and Ryerson University. This study was supported, in part, by the CIHR Excellence in Radiation Research for the 21st century (EIRR21) Research Training Program, the Ontario Institute for Cancer Research Network through funding provided by the Province of Ontario, the FY07 Department of Defense Breast Cancer Research Program Concept Award (BC075873) and a program project grants entitled “Imaging for Cancer” and “Ultrasound for Cancer Therapy” from the Terry Fox Foundation.

#144029 - $15.00 USDv Received 14 Mar 2011; revised 14 Apr 2011; accepted 26 Apr 2011; published 4 May 2011